Nanocrack generation at dislocation-disclination configurations in nanocrystalline metals and ceramics

I. A. Ovid'ko* and A. G. Sheinerman
Institute for Problems of Mechanical Engineering, Russian Academy of Sciences, Bolshoj 61, Vasilievskii Ostrov, St. Petersburg 199178, Russia

(Received 8 August 2007; revised manuscript received 3 December 2007; published 27 February 2008)

A theoretical model is suggested which describes the generation of nanoscale cracks in deformed nanocrystalline metals and ceramics. In the framework of the model, cracks are generated in the superposition of the stress fields of interfacial edge dislocations and disclination dipoles formed at interfaces (grain and interphase boundaries) during plastic deformation of nanocrystalline metals and ceramics. It is theoretically shown that the generation of cracks at such dislocation-disclination configurations is energetically favorable in nanocrystalline Ni and nanoceramics, 3*C*-SiC and α-Al_2O_3, in wide ranges of their structural parameters.

DOI: 10.1103/PhysRevB.77.054109 PACS number(s): 61.72.Lk, 61.72.Mm, 61.72.Bb, 62.20.M−

I. INTRODUCTION

Dislocations—line defects of translational type—represent typical defects strongly influencing the physical and mechanical properties of conventional crystalline and nanocrystalline solids.[1–17] In recent years, wedge disclinations—line defects characterized by rotations of the crystalline lattice around their lines[18]—have attracted considerable interest as imperfections inherent to various nanostructured solids.[19–24] Commonly, wedge disclinations are located at interfaces (grain and interphase boundaries) shared by neighboring misoriented crystallites. In a first approximation, a wedge disclination at an interface is defined as a line defect dividing interface fragments characterized by different tilt misorientation angles. The strength of this wedge disclination represents the difference between the tilt misorientation angles of the interface fragments.

The formation of disclinations is enhanced in nanostructured solids where the volume fraction of interfaces is high and interfacial disclinations are located sufficiently close to each other (or to a free surface) in order to effectively screen their stress fields.[19–24] For instance, disclinations are recognized as typical defects that can strongly influence the physical and mechanical properties of bulk nanocrystalline solids[19–21,24] and nanowires.[22,23]

In particular, as with dislocations that can initiate cracks in conventional polycrystals[25–28] and nanocrystalline solids,[29,30] disclinations create stress fields whose relaxation can occur through crack generation in nanowires,[22,23,31] polycrystalline,[32,33] and nanocrystalline[24] solids. In this context, with the typical coexistence of dislocations and disclinations in nanostructured solids, these defects cause combined effects on crack generation, and, generally speaking, the effects in question do not represent a simple superposition of the separate effects of dislocations and disclinations on crack generation. As a corollary, there is large interest, from both fundamental and applied viewpoints, in the description of crack generation induced by both dislocations and disclinations in nanocrystalline solids. The main aim of this paper is to theoretically describe crack generation at dislocation-disclination configurations formed during plastic deformation in nanocrystalline metals and ceramics.

II. FORMATION OF DISLOCATION-DISCLINATION CONFIGURATIONS AT INTERFACES IN DEFORMED NANOCRYSTALLINE SOLIDS

Plastic deformation in nanocrystalline solids is strongly influenced by interfaces; see, e.g., Refs. 34–36. In particular, grain boundaries hamper intragrain slip carried by lattice dislocations, and triple junctions of grain boundaries hamper intergrain sliding carried by interfacial dislocations and/or local shear events.[37] These hampering effects are, in part, related to the formation of disclination dipoles and dislocations at the places where intragrain slip occurs across grain boundaries and the places where intergrain sliding occurs across triple junctions.

Commonly, disclination dipoles are generated at grain boundaries due to interfacial sliding[24] that dominates, in particular, in superplastic deformation of nanocrystalline metals and ceramics.[34–36] For instance, Fig. 1 schematically shows the transfer of a vertical high-angle tilt boundary (from the position A′A to the position B′B) due to the interfacial sliding along the high-angle boundary AC. In the initial state, the triple junction A of high-angle grain boundaries is supposed to be geometrically balanced. (There is no angle gap at the triple junction A or, in other words, the sum of tilt misorientation angles at this junction is equal to zero.) As a result of the transfer, the angle gaps ω and $-\omega$ appear at the grain boundary junctions A and B, respectively, where ω is the tilt misorientation of the vertical boundary.[24] In the theory of defects in solids, the junctions A and B with the angle gaps $\pm\omega$ represent wedge disclinations which are characterized by the strengths $\pm\omega$ (Refs. 18 and 38) and form a dipole configuration.

Strictly speaking, the two grain boundary junctions A and B [Fig. 1(b)] are equivalent to the disclination dipole in the only approximation that the discrete grain boundary dislocations (whose Burgers vectors belong to the dense-shift-complete lattices of grain boundaries[39]) are spread into a continuous distribution of infinitesimal dislocations. However, this approximation is conventional[18,22–24,31–33] and effective in the considered case of high-angle grain boundaries (Fig. 1), because the discrete character of arrangement of grain boundary dislocations is not commonly essential for

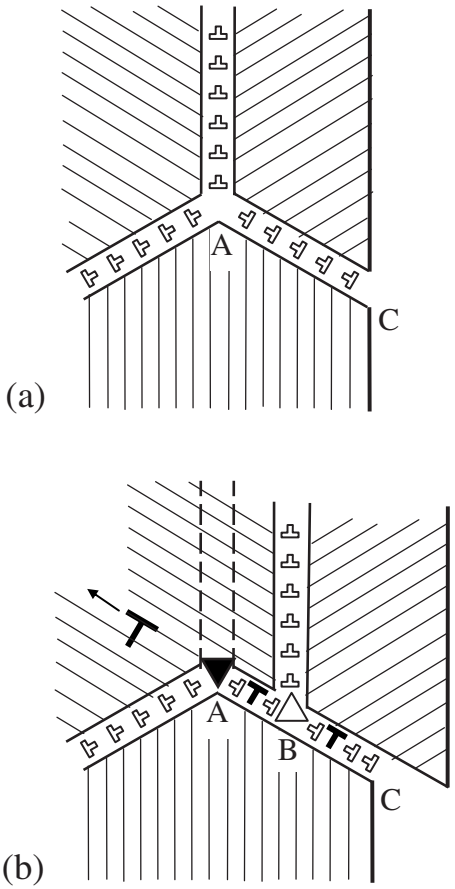

FIG. 1. Formation of a dislocation-disclination configuration in a nanocrystalline solid deformed by intergrain sliding. (a) Initial state. (b) Interfacial sliding across a triple junction of interfaces produces a disclination dipole at an interface fragment along which the triple junction shifts. Also, dislocation charge is accumulated at the interface fragment.

the stress fields of the junctions of high-angle boundaries.

Interfacial sliding across a triple junction is, in part, stopped at the triple junction due to the difficulties in the emission of lattice dislocations from the triple junction. In doing so, the grain boundary fragment AB contains a dislocation or a dislocation pileup associated with the stopped interfacial sliding. (For simplicity, hereinafter, we assume that one dislocation forms at the grain boundary fragment AB and is characterized by a Burgers vector $\boldsymbol{b}$, which is not necessarily a lattice vector.) As a result, a dislocation-disclination configuration is generated that consists of a disclination dipole and a dislocation at the grain boundary fragment AB [Fig. 1(b)].

Thus, dislocation-disclination configurations can form due to the intergrain sliding in deformed nanocrystalline metals and ceramics. Below, we will theoretically examine the role of these configurations in crack nucleation.

III. CONDITIONS FOR ENERGETICALLY FAVORABLE GENERATION OF CRACKS AT INTERFACIAL DISLOCATION-DISCLINATION CONFIGURATIONS

Previous models for the generation of nano-or microcracks in the stress fields of defects in solids have been focused on crack generation events in the stress fields of either dislocations[25–30] or disclinations.[22–24,31–33] In particular, the calculations[31,33] demonstrate that a grain boundary crack formed at a triple junction disclination is favored to grow when the crack length l lies within some interval: $l_{e1}<l<l_{e2}$. The growth of a grain boundary crack in the stress field of a superdislocation is shown to be favorable if the crack length is smaller than some equilibrium length. l_e.[28,29] At the same time, if the stress field of a triple junction superdislocation is partially relieved by intensive grain boundary diffusion,[30] crack growth is favored within some crack length interval, as with the case of a crack generated at a triple junction disclination.

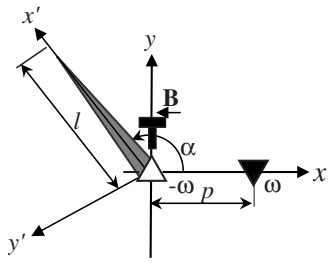

FIG. 2. Formation of a nanocrack at a disclination dipole and dislocation with a large Burgers vector.

In this paper, we consider crack formation in the stress field of both a dislocation with a large Burgers vector and a disclination dipole. It will be demonstrated that in this case, the crack is beneficial to grow until its length is smaller than some equilibrium length l_e, as in the situation of a crack formed at an isolated dislocation. At the same time, the equilibrium length for a crack generated in the stress field of both a dislocation and a disclination dipole is much larger than the equilibrium lengths of the cracks nucleating at an isolated dislocation or an isolated disclination dipole with the same characteristics.

Let us consider a nanocrack generated at an edge dislocation and a dipole of wedge disclinations (Fig. 2). We denote the strengths of the dipole disclinations as $-\omega$ and ω and the dislocation Burgers vector as $\boldsymbol{B}$. Let us introduce a Cartesian coordinate system (x,y), as shown in Fig. 2. In this coordinate system, the disclinations ω and $-\omega$ are assumed to lie at the x axis at the points $x=p$ and $x=0$, respectively, while the edge dislocation is supposed to lie in the origin of the coordinate system (x,y), at the same point as the disclination $-\omega$. The dislocation Burgers vector is assumed to be directed in the direction opposite to the direction of the x axis ($\boldsymbol{B}=-B\boldsymbol{e}_x$).

Let the stress field of the dislocation and disclination dipole induce the formation of a flat nanocrack of length l that makes an angle α with the x axis. (In general, an applied stress also acts in the deformed material. However, for the nanocracks with the lengths up to several tens of nanometers considered in this paper, the effect of an applied stress on crack generation and growth is typically insignificant and can be neglected.) To calculate the conditions for nanocrack formation, we introduce a crack-related coordinate system (x',y') (see Fig. 2) and compute the stresses, $\sigma_{y'y'}(x',y'=0)$ and $\sigma_{x'y'}(x',y'=0)$, created by the disclination dipole

and superdislocation in the nanocrack plane. These stresses are calculated using the expressions for the stress field of a disclination[38] and dislocation[40] in an elastically isotropic infinite solid. The final expressions for the stresses $\sigma_{y'y'}(x',y'=0)$ and $\sigma_{x'y'}(x',y'=0)$ are as follows: $\sigma_{y'y'}(x',y'=0)=Df_1(x')$, $\sigma_{x'y'}(x',y'=0)=-Df_2(x')$, where

$$f_1(x') = \omega\left(\frac{1}{2}\ln\frac{x'^2 - 2px'\cos\alpha + p^2}{x'^2} - \frac{p^2\sin^2\alpha}{x'^2 - 2px'\cos\alpha + p^2}\right) + \frac{B\sin\alpha}{x'}, \tag{1}$$

$$f_2(x') = \frac{\omega p\sin\alpha(x' - p\cos\alpha)}{x'^2 - 2px'\cos\alpha + p^2} + \frac{B\cos\alpha}{x'}, \tag{2}$$

$D=G/[2\pi(1-\nu)]$, G is the shear modulus, and ν is Poisson's ratio.

To estimate the conditions for nanocrack growth, we use the energetic criterion[28,29]

$$F > 2\gamma_e, \tag{3}$$

where F is the energy release rate and γ_e is the effective surface energy. In the considered case of an elastically isotropic solid and plane strain state, the energy release rate F is given as[28]

$$F = \frac{\pi(1-\nu)l}{4G}(\bar{\sigma}^2_{y'y'} + \bar{\sigma}^2_{x'y'}), \tag{4}$$

where $\bar{\sigma}_{y'y'}$ and $\bar{\sigma}_{x'y'}$ are the mean weighted values of the stresses $\sigma_{y'y'}$ and $\sigma_{x'y'}$. The mean weighted stresses $\bar{\sigma}_{y'y'}$ and $\bar{\sigma}_{x'y'}$ are defined as[28]

$$\bar{\sigma}_{my'} = \frac{2}{\pi l}\int_0^l \sigma_{my'}(x',y'=0)\sqrt{\frac{x'}{l-x'}}dx', \quad m = x',y'. \tag{5}$$

The effective surface energy γ_e is equal to $\gamma-\gamma_b/2$ for a grain boundary nanocrack, and to γ for an intragrain nanocrack. Here, γ is the specific surface energy, and γ_b is the energy of a grain boundary per its unit area.

With formulas (4) and (5) substituted to expression (3), we obtain the following necessary condition for nanocrack growth: $q > q_c$, where

$$q = \frac{1}{\sqrt{Bl}}\left[\left(\int_0^l f_1(x)\sqrt{\frac{x}{l-x}}dx\right)^2 + \left(\int_0^l f_2(x)\sqrt{\frac{x}{l-x}}dx\right)^2\right]^{1/2}, \tag{6}$$

$$q_c = \sqrt{\frac{8\pi^3(1-\nu)\gamma_e}{GB}}. \tag{7}$$

In addition to the condition $q > q_c$ of nanocrack growth, there is another condition that the nanocrack is most favorable to be generated in the space area where both the dislocation and the disclination dipole would create zero or tensile normal stresses in the direction perpendicular to the nanocrack plane. The latter condition yields $\pi/2 \leqslant \alpha \leqslant \pi$. Notice that a grain boundary nanocrack can also form outside this region if grain boundaries in this region are absent and the mean weighted normal stress in the direction perpendicular to the nanocrack is positive. However, the region $\pi/2 \leqslant \alpha \leqslant \pi$ is most favorable for nanocrack formation, and the equilibrium lengths of grain boundary nanocracks in this region are larger than those of nanocracks outside this region.

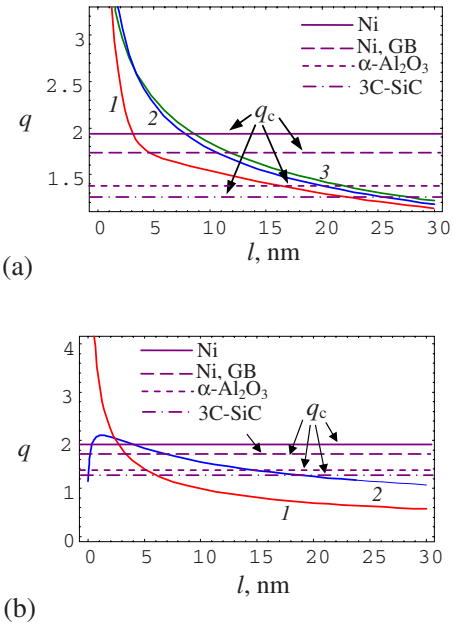

FIG. 3. (Color online) Dependences of the parameter q on the nanocrack length l. (a) $B=1$ nm, $\omega=\pi/4$, $\alpha=\pi/2$, $3\pi/4$, and π (curves 1, 2, and 3, respectively). (b) $B=1$ nm, $\omega=0$, and $\alpha=\pi/2$ (curve 1); $B=0$, $\omega=\pi/4$, and $\alpha=\pi$ (curve 2). The solid and long dashed horizontal lines show the values of the parameter q_c for an intragrain and grain boundary nanocrack in nanocrystalline Ni, respectively. The short dashed and dotted horizontal lines depict the values of the parameter q_c for intragrain nanocracks in nanoceramic α-Al_2O_3 and 3C-SiC, respectively.

The dependences $q(l)$, for $p=3$ nm, $B=1$ nm, $\omega=\pi/4$, and different values of the angle α from the interval $\pi/2 \leqslant \alpha \leqslant \pi$, are presented in Fig. 3(a). The solid and long dashed horizontal lines show the values of the parameter q_c for intragrain and grain boundary nanocracks in nanocrystalline Ni, respectively. The short dashed and dotted horizontal lines show the values of the parameter q_c characterizing intragrain nanocracks in nanocrystalline α-Al_2O_3 (corundum) and 3C-SiC (the cubic phase of silicon carbide), respectively. The values of q_c are calculated for $B=1$ nm and $\omega=\pi/4$. In the case of Ni, we have[40,41] $G=79$ GPa, $\nu=0.31$, $\gamma=1.725$ J/m^2, and $\gamma_b=0.69$ J/m^2. Substitution of the above values of parameters to formula (7) yields $q_c \approx 1.93$, for intragrain nanocrack in Ni, and $q_c \approx 1.73$, for a grain boundary nanocrack in Ni. In the case of α-Al_2O_3 with the characteristic parameter values[42,43] $G=169$ GPa, $\nu=0.23$, and $\gamma=1.69$ J/m^2, we get $q_c \approx 1.38$. Finally, in the case of 3C-SiC with the characteristic parameter values[44] $G=217$ GPa, $\nu=0.23$, and $\gamma=1.84$ J/m^2, we obtain $q_c \approx 1.27$.

The growth of an intragrain (grain boundary, respectively) nanocrack in Ni is energetically favored in the parameter

ranges where the curves $q(l)$ lie higher than the solid (long dashed, respectively) horizontal line. The growth of an intragrain nanocrack in α-Al_2O_3 ($3C$-SiC, respectively) is energetically beneficial in the parameter ranges where the curves $q(l)$ lie higher than the short dashed (dotted, respectively) horizontal line. As it follows from Fig. 3(a), nanocrack growth is energetically favorable if the nanocrack length is smaller than some equilibrium length l_e. The equilibrium length l_e is determined by the point of intersection of the curve $q(l)$ with the corresponding horizontal line. In the most favorable case for nanocrack growth, where α is close to π [see curve 3 in Fig. 3(a)], we have $l_e \approx 9$ nm, for an intragrain nanocrack in Ni, $l_e \approx 12$ nm, for a grain boundary nanocrack in Ni, $l_e \approx 22$ nm, for an intragrain nanocrack in α-Al_2O_3, and $l_e \approx 27$ nm, for an intragrain nanocrack in $3C$-SiC. The values of l_e for an intragrain nanocracks in α-Al_2O_3 and $3C$-SiC are much larger than the values of l_e for both intragrain and grain boundary nanocracks in Ni. The large values of l_e for α-Al_2O_3 and $3C$-SiC (compared to the case of Ni) are associated with low values of the ratio γ/G for these materials, which controls the initiation and propagation of brittle cracks.

Thus, dislocation-disclination configurations create high local stresses. These stresses are capable of causing the energetically favorable formation of a crack with the length of several nanometers in deformed nanocrystalline metals and ceramics.

IV. COMPARISON OF CONDITIONS FOR CRACK GENERATION AT DISLOCATION-DISCLINATION CONFIGURATIONS, ISOLATED DISLOCATION, AND ISOLATED DISCLINATION DIPOLE

Let us compare the conditions for the energetically favorable generation of cracks at dislocation-disclination configurations, isolated dislocation, and isolated disclination dipole. Figure 3(b) shows the dependences $q(l)$ in the the cases where the nanocrack nucleates in the stress field of either a dislocation (without a disclination dipole) or a disclination dipole (without a dislocation). In both cases, the curves $q(l)$ in Fig. 3(b) are plotted for the most favorable situation (for crack nucleation and growth) where the normal tensile stress in the direction perpendicular to the crack plane is maximum. This corresponds to $\alpha=\pi/2$, for the crack nucleating at a dislocation, and to $\alpha=\pi$, for the crack generated at a disclination dipole. As it follows from Fig. 3(b), in the case where a crack nucleates at an isolated dislocation with a large Burgers vector [see curve 1 in Fig. 3(b)], it is favored to grow until the crack length is smaller than its equilibrium length. In the case where a crack nucleates at an isolated disclination dipole [see curve 2 in Fig. 3(b)], it is, in general, favored to grow within a crack length interval $l_c<l<l_e$, where the lengths l_c and l_e are given by the points of the intersection of curve 2 in Fig. 3(b) with the corresponding horizontal line. In this general case, crack propagation in the interval $l<l_c$ requires thermal fluctuations while its advance in the interval $l_c<l<l_e$ is characterized by the absence of any energy barrier. However, for large enough values of the disclination strength ω and/or dipole arm p, the critical crack length l_c is smaller than or comparable with the interatomic distance. [This case is shown in Fig. 3(b).] In these circumstances, the crack can grow in the nonbarrier way within the crack length interval $0<l<l_e$, as with the case of a crack that nucleates at a dislocation.

Comparison of Figs. 3(a) and 3(b) shows that the equilibrium lengths of the nanocracks generated either at a dislocation with the Burgers vector magnitude $\boldsymbol{B}$ or at a disclination dipole with the disclination strength ω [see Fig. 3(b)] are smaller than the equilibrium length of a crack nucleating in the stress field of both such a dislocation and such a disclination dipole [see Fig. 3(a)]. That is, the combined effect of a dislocation and a disclination dipole on crack generation is stronger than the separate effects of either an isolated dislocation or an isolated disclination dipole with the same characteristics.

V. EFFECT OF DISCRETE DISLOCATION STRUCTURE OF GRAIN BOUNDARIES ON CRACK GENERATION

Besides high-angle grain boundaries, low-angle boundaries serve as typical structural elements in nanostructured solids. For instance, many low-angle tilt boundaries are present in nanocrystalline metals fabricated by high-pressure torsion[45] and cryomilling method.[46] During the slip of lattice dislocations across low-angle tilt boundaries, boundary steps form which contain specific defect configurations.[47,48] In particular, dislocation configurations (Fig. 4) can form at low-angle boundaries, which are very similar to disclination-dislocation configurations [Fig. 1(b)] generated at high-angle tilt boundaries due to the intergrain sliding. At the same time, the dislocation configurations [Fig. 4(b)] have their specific features related to the dislocation structure of low-angle tilt boundaries. Such boundaries represent lattice dislocation walls[39,49] whose discrete structure is essential for adequate description of its stress field near the walls. For instance, we consider the initial low-angle tilt boundary [Fig. 4(a)] which is cut by the lattice dislocation slip across its plane into two straight dislocation wall segments displaced relative to each other, as shown in Fig. 4(b). The sum stress field of the dislocation wall segments approaches the stress field of a disclination dipole at large enough distances from these segments but differs from the stress field of such a dipole near the segments. Therefore, in examination of crack nucleation near the low-angle tilt boundary step, it is not always reasonable to use the approximation that the discrete dislocations are spread into a continuous distribution of infinitesimal dislocations.

In this section, we will examine the conditions for the nucleation of a crack at the discrete dislocation configuration formed during the slip of lattice dislocations across a low-angle tilt boundary (Fig. 4). To do so, we will model the discrete dislocation configuration as resulting from the split of an infinite wall of lattice edge dislocations into two semi-infinite dislocation walls (Fig. 5). We will also suppose that some of gliding dislocations pass through the grain boundary while others are stopped at the boundary step (because an increase in the step height p is hampered by the corresponding increase in the elastic energy of the semi-infinite dislo-

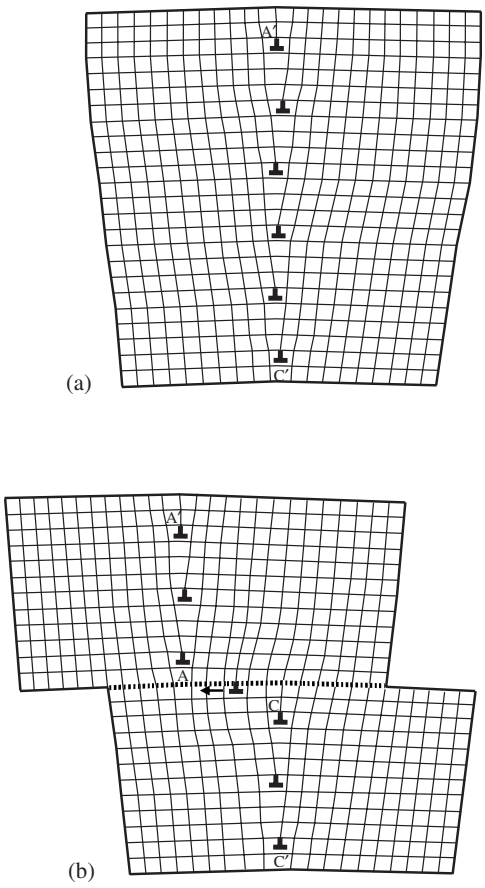

FIG. 4. Formation of a dislocated step at a low-angle tilt boundary due to the slip of lattice dislocations across the boundary plane.

cation walls). For the sake of simplicity, we model the dislocations stopped at the boundary step as one dislocation with a large Burgers vector $\boldsymbol{B}$. We also denote the Burgers vectors of lattice dislocations that form dislocation walls as $\boldsymbol{b}$ and the distance between neighboring dislocations in the walls as h. The magnitude b of the dislocation Burgers vectors and the dislocation separation in the walls h are related to the misorientation ω of the stepped grain boundary (modeled by dislocation walls) by the approximate relation $\omega \approx b/h$. The dislocation with a large Burgers vector $\boldsymbol{B}$ is assumed to lie between the dislocation walls, at the distance $p/2$ from both walls. In the coordinate system of Fig. 5, the

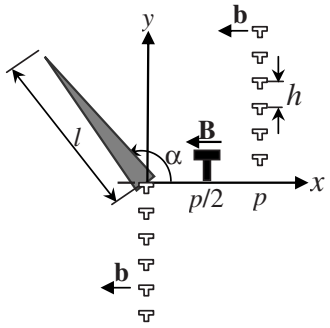

FIG. 5. Formation of a nanocrack at a dislocation wall step containing a dislocation with a large Burgers vector.

dislocations that compose the walls have Burgers vectors $-b\boldsymbol{e}_x$ while the dislocation with a large Burgers vector has the Burgers vector $-B\boldsymbol{e}_x$. The dislocations that belong to the walls are located at the points $[x=0,\ y=-(n-1)h]$ and $(x=p,\ y=nh)$, where $n=1,2,\ldots,\infty$. The dislocation with a large Burgers vector lies at the point $(x=p/2,\ y=0)$. The crack, if it forms, has a length l and grows along the plane that makes an angle α with the x axis.

Based on the above assumptions, we calculate the conditions for the energetically favorable nanocrack nucleation and growth. To do so, we use a slightly modified version of the calculation procedure employed in Sec. III. The modification is in the use of the expressions for the stress fields of edge dislocations forming wall configurations instead of the expressions for the stress fields of a disclination dipole. As a result, after some algebra, we find the following condition for the energetically favorable growth of the nanocrack: $\tilde{q} > \tilde{q}_c$, where

$$q_c = \sqrt{\frac{8\pi^3(1-\nu)\gamma_e}{GB}}, \tag{8}$$

$$\tilde{q} = \frac{1}{\sqrt{bl}}\left[\left(\int_0^l g_{xy}^t(x)\sqrt{\frac{x}{l-x}}dx\right)^2 + \left(\int_0^l g_{yy}^t(x)\sqrt{\frac{x}{l-x}}dx\right)^2\right]^{1/2}, \tag{9}$$

$$g_{my}^t(x) = (B/b)g_{my}(p/2,0,x) + \sum_{n=1}^{\infty}[g_{my}(0,-(n-1)b/\omega,x) + g_{my}(p,nb/\omega,x)], \tag{10}$$

$$g_{xy}(x_0,y_0,x) = \frac{\tilde{x}[2\tilde{x}\tilde{y}\sin 2\alpha + (\tilde{x}^2-\tilde{y}^2)\cos 2\alpha]}{\tilde{r}^4}, \tag{11}$$

$$g_{yy}(x_0,y_0,x) = \frac{\tilde{y}(2\tilde{x}^2\cos 2\alpha - \tilde{r}^2) - \tilde{x}(\tilde{x}^2-\tilde{y}^2)\sin 2\alpha}{\tilde{r}^4}, \tag{12}$$

$m=x,y$, $\tilde{x}=x\cos\alpha - x_0$, $\tilde{y}=x\sin\alpha - x_0$, and $\tilde{r}^2=\tilde{x}^2+\tilde{y}^2$.

The dependences $q(l/b)$, for $p=6$ nm, $B=1$ nm, $\omega=\pi/18=10°$, and different values of the angle α from the interval $\pi/2 \leqslant \alpha \leqslant \pi$, are presented in Fig. 6. The maximum value of $\tilde{q}$ for these parameter values is about 1.8. Analysis shows that, even for the large height of the grain boundary step ($p=6$ nm), this value (1.8) is much less than typical values of $\tilde{q}_c$ for metals. For example, for intragrain and grain boundary nanocracks in nanocrystalline Ni, characterized by $b=0.25$ nm and the values of other parameters specified above, we obtain $\tilde{q}_c \approx 3.86$ and $\tilde{q}_c \approx 3.45$, respectively. This means that the relation $\tilde{q} > \tilde{q}_c$ of nanocrack growth is not met for any nanocrack length. Therefore, the formation of nanocracks at the dislocated steps of low-angle tilt boundaries is not likely.

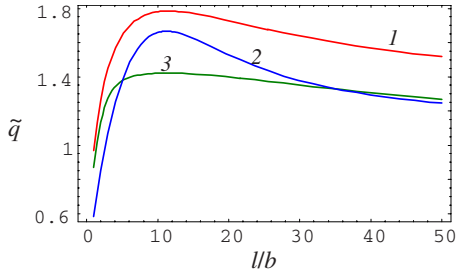

FIG. 6. (Color online) Dependences of the parameter $\tilde{q}$ on the normalized nanocrack length l/b, for $B=1$ nm, $\omega=\pi/18$, $\alpha=3\pi/4$, $\pi/2$, and π (curves 1, 2, and 3, respectively).

VI. CONCLUDING REMARKS

Thus, following the results of the theoretical analysis given in this paper, dislocation-disclination configurations effectively form in the vicinity of triple junctions that move due to the intergrain sliding in nanocrystalline solids (Fig. 1). Dislocation-disclination configurations serve as powerful stress sources capable of initiating nanoscale cracks in deformed nanocrystalline metals and ceramics. In particular, our calculations and estimates have shown that the generation of cracks is energetically favorable in deformed nanocrystalline Ni, α-Al_2O_3, and $3C$-SiC in wide ranges of their structural parameters. The enhanced formation of cracks at dislocation-disclination configurations (formed in the vicinity of triple junctions that move due to intergrain sliding) is in agreement with the experimental observation of nanoscale cracks at the triple junctions of grain boundaries in nanocrystalline Ni (Ref. 50) and cracks at the interfaces between the large grains and nanocrystalline matrix in nanomaterials with a bimodal structure.[51]

The enhancing effect of dislocation-disclination configurations on crack formation decreases ductility of nanocrystalline solids. In general, the effect in question can be diminished or even suppressed by intensive relaxation processes—diffusion and lattice dislocation emission from grain boundaries—releasing, in part, the stresses of dislocation-disclination configurations. In this case, crack generation is hampered, and a nanocrystalline solid tends to show the ductile behavior.

ACKNOWLEDGMENTS

This work was supported, in part, by the Office of US Naval Research (Grant No. N00014-07-1-0295), Russian Academy of Sciences Program "Structural Mechanics of Materials and Construction Elements," Russian Federal Agency of Science and Innovations (Contract 02.513.11.3190 of the Program "Industry of Nanosystems and Materials"), CRDF (Grant No. RUE2-2684-ST-05), and St. Petersburg Center of the Russian Academy of Sciences.

*Author to whom correspondence should be addressed; ovidko@def.ipme.ru

[1] A. El-Azab, Phys. Rev. B **61**, 11956 (2000).
[2] M. Zaiser, M. Carmen Miguel, and I. Groma, Phys. Rev. B **64**, 224102 (2001).
[3] I. A. Ovid'ko, Phys. Rev. Lett. **88**, 046103 (2002).
[4] I. A. Ovid'ko and A. G. Sheinerman, Phys. Rev. B **66**, 245309 (2002).
[5] J. Coelho, G. Patriarche, F. Glas, G. Saint-Girons, I. Sagnes, and L. Largeau, Phys. Rev. B **70**, 155329 (2004).
[6] D. Sherman and I. Be'ery, Phys. Rev. Lett. **93**, 265501 (2004).
[7] S. G. Srinivasan, X. Z. Liao, M. I. Baskes, R. J. McCabe, Y. H. Zhao, and Y. T. Zhu, Phys. Rev. Lett. **94**, 125502 (2005).
[8] T. Shimokawa, A. Nakatani, and H. Kitagawa, Phys. Rev. B **71**, 224110 (2005).
[9] F. Glas, Phys. Rev. B **74**, 121302(R) (2006).
[10] S. V. Bobylev, M. Yu. Gutkin, and I. A. Ovid'ko, Phys. Rev. B **73**, 064102 (2006).
[11] I. A. Ovid'ko and A. G. Sheinerman, Adv. Phys. **55**, 627 (2006).
[12] I. N. Remediakis, D. E. Jesson, and P. C. Kelires, Phys. Rev. Lett. **97**, 255502 (2006).
[13] S. Limkumnerd and J. P. Sethna, Phys. Rev. Lett. **96**, 095503 (2006).
[14] D. Mordehai, I. Kelson, and G. Makov, Phys. Rev. B **74**, 184115 (2006).
[15] J. C. M. Li, Phys. Rev. Lett. **96**, 215506 (2006).
[16] Z. W. Shan, J. M. K. Wiezorek, E. A. Stach, D. M. Follstaedt, J. A. Knapp, and S. X. Mao, Phys. Rev. Lett. **98**, 095502 (2007).
[17] J. C. M. Li, Appl. Phys. Lett. **90**, 041912 (2007).
[18] A. E. Romanov, Eur. J. Mech. A/Solids **22**, 727 (2003).
[19] M. Murayama, J. M. Howe, H. Hidaka, and S. Takaki, Science **295**, 2433 (2002).
[20] I. A. Ovid'ko, Science **295**, 2386 (2002).
[21] M. Yu. Gutkin and I. A. Ovid'ko, Appl. Phys. Lett. **87**, 251916 (2005).
[22] K. Zhou, A. A. Nazarov, and M. S. Wu, Phys. Rev. B **73**, 045410 (2006).
[23] K. Zhou, A. A. Nazarov, and M. S. Wu, Phys. Rev. Lett. **98**, 035501 (2007).
[24] I. A. Ovid'ko and A. G. Sheinerman, Appl. Phys. Lett. **90**, 171927 (2007).
[25] C. Zener, in *Fracturing of Metals*, edited by F. Jonassen, W. P. Roop, and R. T. Bayless (American Society of Metals, Cleveland, OH, 1948), p. 3.
[26] J. S. Koehler, Phys. Rev. **85**, 480 (1952).
[27] A. N. Stroh, Proc. R. Soc. London, Ser. A **223**, 404 (1954).
[28] V. I. Indenbom, Sov. Phys. Solid State **3**, 1506 (1961).
[29] I. A. Ovid'ko and A. G. Sheinerman, Acta Mater. **52**, 1201 (2004).
[30] I. A. Ovid'ko and A. G. Sheinerman, Acta Mater. **53**, 1347 (2005).
[31] M. S. Wu and H. Zhou, Int. J. Fract. **82**, 381 (1996).
[32] V. V. Rybin and I. M. Zhukovskii, Fiz. Tverd. Tela (Leningrad) **20**, 1829 (1978) [Sov. Phys. Solid State **20**, 1056 (1978)].
[33] M. Yu. Gutkin and I. A. Ovid'ko, Philos. Mag. A **70**, 561 (1994).
[34] D. Wolf, V. Yamakov, S. R. Phillpot, A. K. Mukherjee, and H.

Gleiter, Acta Mater. **53**, 1 (2005).
[35] M. A. Meyers, A. Mishra, and D. J. Benson, Prog. Mater. Sci. **51**, 427 (2006).
[36] C. Koch, I. A. Ovid'ko, S. Seal, and S. Veprek, *Structural Nanocrystalline Materials: Fundamentals and Applications* (Cambridge University Press, Cambridge, 2007).
[37] H. Conrad and J. Narayan, Scr. Mater. **42**, 1025 (2000).
[38] A. E. Romanov and V. I. Vladimirov, in *Dislocations in Solids*, edited by F. R. N. Nabarro (North-Holland, Amsterdam, 1992), Vol. 9, p. 191.
[39] A. P. Sutton and R. W. Balluffi, *Interfaces in Crystalline Materials* (Clarendon, Oxford, 1995).
[40] J. P. Hirth and J. Lothe, *Theory of Dislocations* (Wiley, New York, 1982).
[41] C. J. Smithells and E. A. Brands, *Metals Reference Book* (Butterworth, London, 1976).
[42] R. G. Munro, J. Am. Ceram. Soc. **80**, 1919 (1997).
[43] Z. Lodziana and J. K. Norskov, J. Chem. Phys. **115**, 11261 (2001).
[44] Z. Ding, S. Zhou, and Y. Zhao, Phys. Rev. B **70**, 184117 (2004).
[45] X. Z. Liao, Y. H. Zhao, Y. T. Zhu, R. Z. Valiev, and D. V. Gundarev, J. Appl. Phys. **96**, 636 (2004).
[46] S. Zghal, M. J. Hytch, J.-P. Chevalier, R. Twesten, F. Wu, and P. Bellon, Adv. Mater. (Weinheim, Ger.) **50**, 4695 (2002).
[47] J. P. Hirth, R. C. Pond, and J. Lothe, Acta Mater. **54**, 4237 (2006).
[48] J. P. Hirth, R. C. Pond, and J. Lothe, Acta Mater. **55**, 5428 (2007).
[49] W. T. Read and W. Schockley, Phys. Rev. **78**, 275 (1950).
[50] K. S. Kumar, S. Suresh, M. F. Chisholm, J. A. Horton, and P. Wang, Acta Mater. **51**, 387 (2003).
[51] B. Q. Han, E. Lavernia, and F. A. Mohamed, Rev. Adv. Mater. Sci. **9**, 1 (2005).